6ICEGE 6th International Conference on Earthquake Geotechnical Engineering
1-4 November 2015
Christchurch. New Zealand

The Role of Ground Motion Characters on the Dynamic Performance of Propped Retaining Structures

F.M. Soccodato[1], G. Tropeano[2]

ABSTRACT

The paper presents the main results of a number of numerical dynamic analyses of propped embedded retaining structures in the time domain. The numerical model entails the static condition of an excavation 4 m height in presence of a pair of retaining cantilever walls in a dry, coarse-grained soil. Afterwards, two structural elements (props) connecting the two opposite walls have been introduced. Four recorded strong-motion acceleration time histories, and four equivalent analytical wavelets, characterized by frequency content rather different have been applied to the bottom of the model. The analyses were carried out considering different maximum accelerations, by scaling the dynamic input. A nonlinear hysteretic soil model coupled with a Mohr-Coulomb strength rule has been adopted. The results of the analyses show the role played by a number of parameters that characterize the seismic signal and the effects of the seismic response on the increment of forces acting on structural elements.

Introduction

The behaviour under seismic condition of embedded, flexible retaining structures is quite complex. Furthermore, data obtained from experimental studies on physical models refer generally to cantilevered walls or with a single level of prop at the top of the wall (Conti et al., 2012). In these cases, it is possible the formation of an instantaneous kinematic mechanism (rigid motion) due to the complete mobilization of the soil resistance, both behind and in front of the wall. Under these conditions, seismic energy is dissipated in the accumulation of permanent displacements of the structure, due to plastic soil straining. The phenomenon can be interpreted in the framework of the displacements methods (rigid-block model), by evaluating the critical acceleration that triggers the collapse mechanism (Callisto and Soccodato, 2010).

When the geometry of the levels of props prevents the formation of kinematic mechanisms and the structural elements do not achieve the yield strength conditions, permanent displacements are expected to be relatively low and, therefore, seismic actions may cause significant increases of the forces acting on the structures: these forces are dependent on a number of factors such as the characteristics of the ground motion, the problem geometry, the mechanical behaviour of the soil and the soil-structure relative stiffness.

In the literature there are several relationships, mainly based on a visco-elastic model for the soil, for the evaluation of maximum seismic stresses acting on retaining walls (Wood, 1973; Veletsos Younam, 1994; Klokinas et al, 2012). These solutions, that are representative of rigid retaining walls, are often used in design practice also in the case of flexible and embedded retaining walls, neglecting the important role played by the part of the structure embedded into the soil and by

[1]Associate Professor,DICAAR, University of Cagliari, Cagliari, Italy, soccodato@unica.it
[2]Assistant Professor, DICAAR, University of Cagliari, Cagliari, Italy, giuseppe.tropeano@unica.it

the global dynamic response of the system.

In this study the preliminary results of a set of dynamics numerical analyses of a pair of multi-propped, embedded retaining walls, in a dry coarse-grained soils are presented and interpreted, with the aim to furnish a contribution to the understanding of the behaviour of this kind of structures under seismic loading.

Numerical Model

Soil Model

The parametric analyses have been carried out with reference to a soil model already considered by Callisto and Soccodato (2007, 2010) and Tropeano and Soccodato (2014). In particular, it consists of a layer of dry coarse-grained soil, 30 m in thickness, resting upon a rigid bedrock. An elastic perfectly plastic model with Mohr-Coulomb strength rule, characterized by mechanical properties corresponding to those of a loose sand (Table 1) was adopted. The shear stiffness at small strains, G_0, is calculated as a function of mean effective stress, p', with the relation:

$$G_0 / p_{ref} = K_G \left(p' / p_{ref} \right)^{0.5} \tag{1}$$

where p_{ref} is a reference pressure (100 kPa) and K_G is a stiffness coefficient set equal to 1000. The soil hysteretic behavior was modeled using the shear modulus decay curves for sands given by Seed and Idriss (1970). The hysteretic damping is, however, computed by applying the generalized Masing criteria implemented in the computer code used in this study.

Table 1. Main soil parameters.

Parameter	Density ρ [Mg/m^3]	Cohesion, c' [kPa]	Friction angle, φ' [°]	At rest earth pressure coefficient, K_0	Poisson ratio, ν'
Value	2.04	0.5	30	0.5	0.2

Seismic Input

The acceleration time histories used in the dynamic analyses (Fig. 1a) are records of strong-motion earthquakes, mainly of Italian events. They are characterized by different frequency content (Fig. 1b, c, d and e) but about the same Arias intensity value ($I_A \approx 0.75$ m/s).

The recordings (S01) have been corrected with a low-pass filter at the cut-off frequency of 15 Hz; additional seismic inputs were obtained by scaling of about 0.7 (S02) and 0.40 (S03) the reference recordings S01. In order to evaluate the effects of the number of cycles on the global response of the system, two simple analytical signals have been also considered. The analytical waveforms correspond to the impulse peak of the recorded accelerograms and they were defined by Ricker wavelet-beta type (R) (one cycle) and Morlet wavelet (M) (two cycles), with a frequency content comparable with that one prevailing in the Fourier spectra of recorded accelerograms (blue and red lines in Figure 1b, c, d and e). Note that M waveforms have a bandwidth narrower than R waveforms.

(a)

ID	Earthquake (date, magnitude M_w)	Station (*rec. comp.*)	a_{max} [g]
TMZ-E	Friuli (06/05/1976, 6.5)	Tolmezzo (NS)	0.350
GLR-E	Loma Prieta (18/10/1989, 6.9)	Gilroy #1 (NS)	0.440(1)
ASS-E	Umbria-Marche 2nd (26/09/1997, 6.0)	Assisi (NS)	0.275
NCR-E	Umbria-Marche 3rd (06/10/1997, 5.4)	Nocera Umbra (WE)	0.330(2)

(1) Scaled to 0.9; (2) Scaled to 1.1.

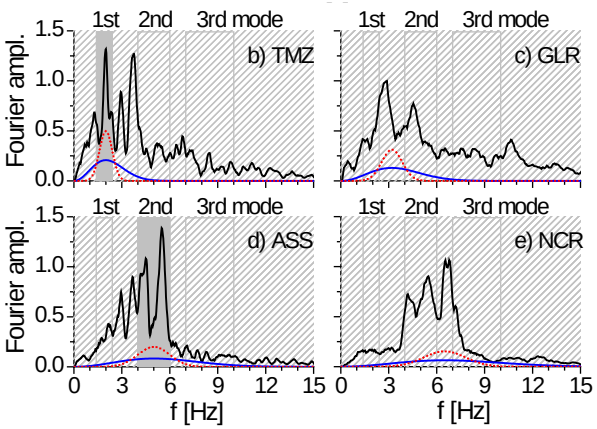

Figure 1. List of acceleration time history S01 (a) and seismic signals in frequency domain (b, c, d and e) of waveforms used in this study.

Schematization and Computational Stages

Numerical dynamic analyses were carried out, under plane strain conditions, with the finite difference code FLAC (Itasca, 2007). The geometry and the computation grid are shown in Figure 2. The pair of walls (L = 8 m) sustains an excavation of height H = 4 m and width 16 m.

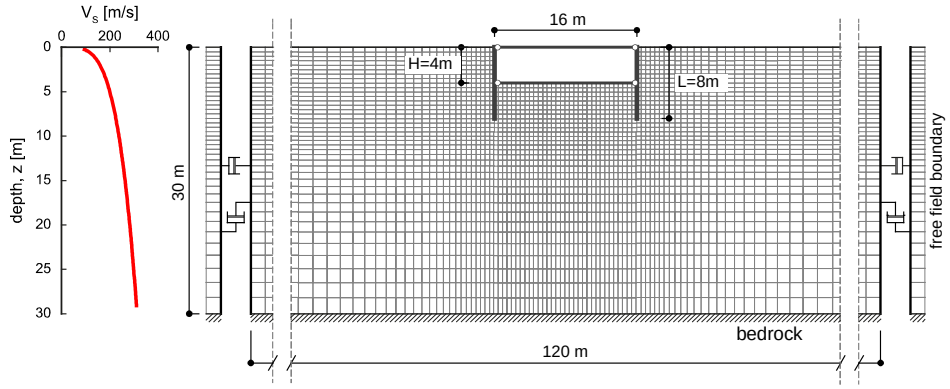

Figure 2. Model geometry and mesh for 2D analyses.

The maximum size of computation mesh elements has been fixed in order to allow the correct propagation of harmonics with a 15Hz maximum frequency, which is the maximum frequency of the seismic signals adopted in this study, according to the well-known indications by Lysmer and Kuhlemeyer (1973). To minimize reflection effects on vertical lateral boundaries of the grid, free field boundary conditions available in FLAC library have been used.

The geotechnical and structural design of walls was managed with reference to the cantilever configuration, assuming this condition as temporary. The permanent levels of props, at the wall top and at the bottom of the excavation, were introduced at the end of the static excavation stages, before the dynamic stage of the analysis.

In detail, walls are supposed to be constituted by reinforced concrete piles 0.6 m in diameter, with spacing equal to 0.7 m: linear elastic beam elements with bending stiffness, *EI*, equal to 2.7×10^5 kN m^2/m were used.

The contact between soil and walls was modelled by using elastic-perfectly plastic interface elements, with a friction angle $\delta = 20°$. As it will be shown in the following, the maximum bending moment in the static cantilevered condition was found to be equal to 90 kNm/m, requiring a yielding moment of the cross section of about 180 kNm/m in order to satisfy Ultimate and Serviceability Limit State checks. Permanent props (r.c. slabs) were also modelled by using beam elements, with axial stiffness, *EA*, equal to 1.0×10^6 kN/m; a pin (zero moment) connection was introduced between prop and wall.

The numerical analysis consisted of the simulation of two main stages:
static stages: wall installation and soil removal until the final excavation depth (4 m) is reached;
dynamic analysis of soil-structure system subjected to seismic loading, after the installation of props.

Results

Ground Motion

The characters of ground motion obtained from the analyses appear greatly affected by a number of overlapping effects:

1. heterogeneity of the soil stiffness profile;
2. non-linearity of soil behaviour;
3. geometry of the system (2D effects);
4. soil-structure interaction.

The comparison between the values of the seismic input parameters and those calculated at ground level allows an estimate of the magnitude of the seismic actions with reference to the effects (1) and (2) above cited. The analysis of the free field motion is summarized in Figure 3a in terms response factors, both using the acceleration ratio (i.e. the ratio of maximum acceleration at ground surface, $a_{\max,FF}$, and maximum acceleration of input record, $a_{\max}$) and the Arias intensity ratio ($I_{A,FF}/I_A$). For the waveforms with a significant high frequency content (ASS and NCR), the free field analysis shows larger amplification of the peak acceleration.

The different soil response is related to the vibration modes excited by the signals. In fact, due to the highly non-linear soil behaviour, the fundamental periods of the soil column appear to be strongly influenced by soil motion and straining (shaded bandwidths in Fig. 1b, c, d and e).

It may be noted that the TMZ waveforms (recorded acceleration time history, E-TMZ, and analytical wavelet, W-TMZ and M-TMZ) gives rise to soil resonance with the first vibration mode (Fig. 1b), which leads to increasing shear strain in the deeper soil layers, and, consequently, additional damping according to the strongly non-linear soil behaviour. As shown in Figure 1d, it is possible to verify that the frequency content of ASS waveforms excites the

system in the second vibration mode, in which the transient deformations and, thus, the associated hysteretic damping, are lesser than for the first mode. NCR and GLR signals have significant frequency content in the second mode bandwidths (except the wavelet M-GLR).

In order to assess the effects (3) and (4), it has been used a synthetic response parameter defined as the ratio between the maximum acceleration at the 2D model surface, $a_{max,S}$, and the peak acceleration at the surface evaluated in free field conditions, $a_{max,FF}$ (Fig. 3c,d and e). The model geometry produces, overall, seismic motion amplification behind the walls and at the excavation center, due to focusing phenomena of the waves, and seismic motion attenuation in front of the wall related to diffraction phenomena of seismic waves.

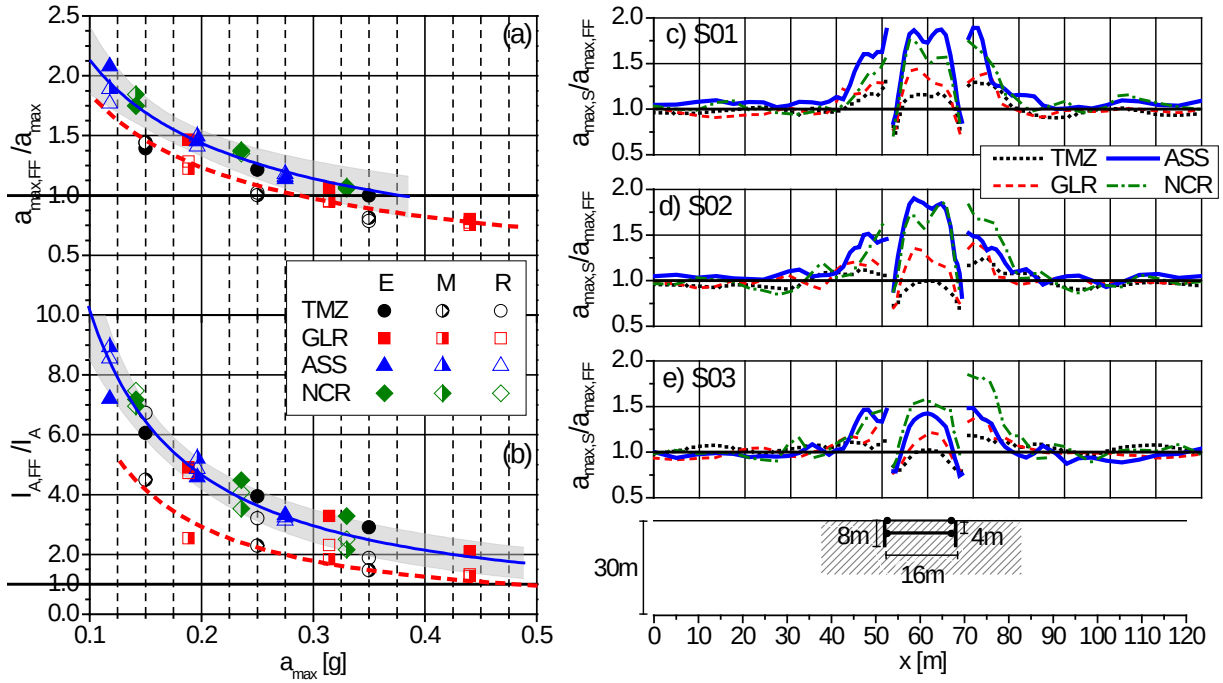

Figure 3. 1D response factors: maximum acceleration (a) and Arias intensity (b). 2D surface response factor for (scaled) earthquake records: S01 (c), S02 (d) and S03(e).

Soil-structure interaction effects produce additional reflections, due to the high stiffness of the walls. The interaction of reflected and incident wave fields modifies the shaking amplitude that depends on the phase shift of the two signals. Both the geometrical amplification and the phase shift are linked to the signal frequency, which is variable according to the nonlinear soil behaviour.

Behaviour of Structures

The presence of the two levels of props connecting the walls greatly influences the behaviour of the structure under seismic loading. In fact, if an elastic behaviour of the structures (walls and props) is assumed, any instantaneous rigid body act of motion associated to a full soil strength mobilization is prevented. In this case, wall deflections and relative displacements are very low;

a significant increase of forces acting on structures is thus expected.
During seismic loading, forces on structures vary rapidly in both magnitude and sign. Typically, for a given time instant, horizontal stresses, σ_h, acting on the two walls are quite different as in the example shows in Figure 4a for the case E-ASS-S01. At this time instant, the horizontal stresses (red lines and symbols) acting behind the left wall reach the maximum values; they are significantly greater than those attained at the end of the static stage (black lines and symbols), in which almost full active limit state conditions were reached. In front of the wall, stresses also increase, and passive limit state conditions extend to a greater depth. Behind the opposite (right) wall, horizontal stresses show a moderate increment in respect of the static condition, while they decrease significantly in front of the wall: this wall seems to be loaded mainly by the bottom strut. The resulting actions on structural elements (bending moments, M, and axial load, N) at this instant of time are shown in Figure 4b. The upper prop is nearly unloaded, and the maximum bending moment, M_{max}, which is about two times the maximum static moment, is reached in correspondence of the lower prop.

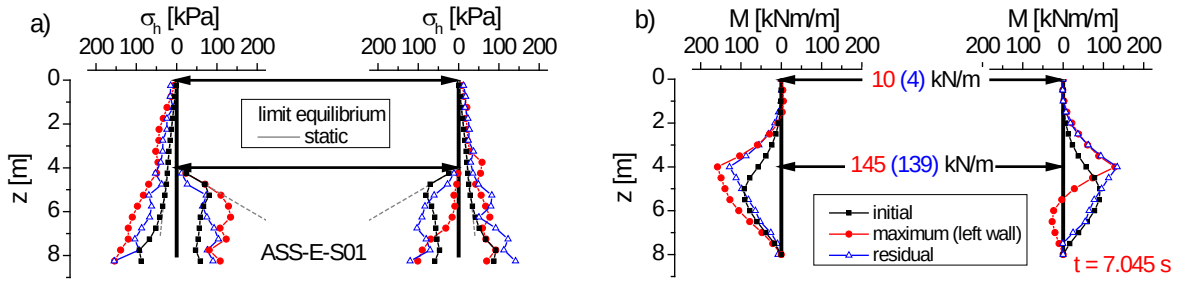

Figure 4. Horizontal stress, σ_h (a), and resulting actions on structural elements (bending moments, M, and axial load, N) (b) for time history E-ASS-S01.

During the main shaking stage, both loads and stresses distributions on the two walls are therefore asymmetric, while in the post-seismic condition they tend to balance (blue lines and symbols in Figure 4). Taking as a reference the static state, the maximum increments of bending moment during the earthquake, ΔM_{max}, and in the post-seismic condition, ΔM_{res}, are attained, for all the seismic input considered, at the elevation of the bottom prop.

Figure 5 shows the time history of the bending moment acting on this section for E-ASS-S01 and E-TMZ-S01 input. Starting from the static value, M_{stat}, bending moment, on the average, appears to increases with time following a trend similar to the Arias Intensity function (red line) up to the final post-seismic value, M_{res}.

Maximum (and minimum) instantaneous bending moments may be considered as deviations from this average baseline trend. Results shows in Figure 5a are typical for seismic input or waveforms with a significant frequency content in the resonant range of the second vibration mode; for the other signals, and in particular for R and M wavelets, the difference between the baseline of bending moments (blue line) and the Arias Intensity function (red line) tend to decrease after the time instant for which the maximum bending moment is reached.

For the post-seismic state, the increment of structural forces appears to be most related to the

ratio T_s^*/T_m (where T_s^* is the fundamental period of the soil column with height equal to the wall length H and T_m is the mean period) to the number of equivalent loading cycles, n_{eq} (defined as the ratio of the significant duration, $D_{5\text{-}95}$, and to the Arial Intensity at ground surface in free field condition, $I_{A,FF}$. The latter parameter, moreover, is more efficient than the other intensity parameters considered ($a_{\max}$, and Housner Intensity, I_H) i.e. it gives the minimum dispersion, σ, in the multivariate regression of data, according to the definition of 'efficiency' in Performance-Based Design framework (Tothong and Luco, 2007) (Figs. 6a and 7a).

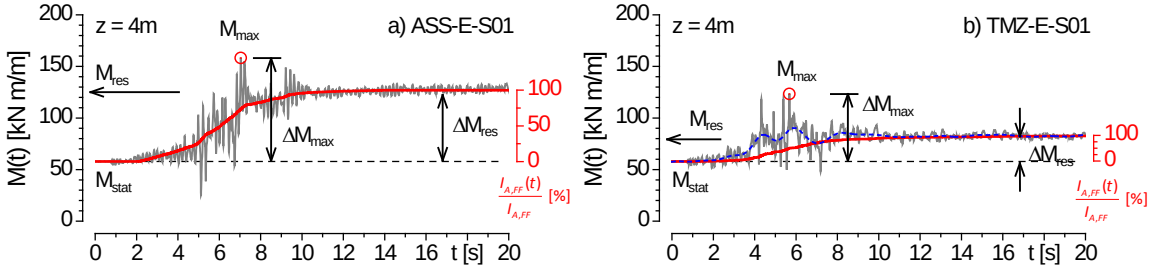

Figure 5. Time history of bending moments at the section corresponding to the lower prop obtained for E-ASS-S01 (a) and E-TMZ-S01 (b) input.

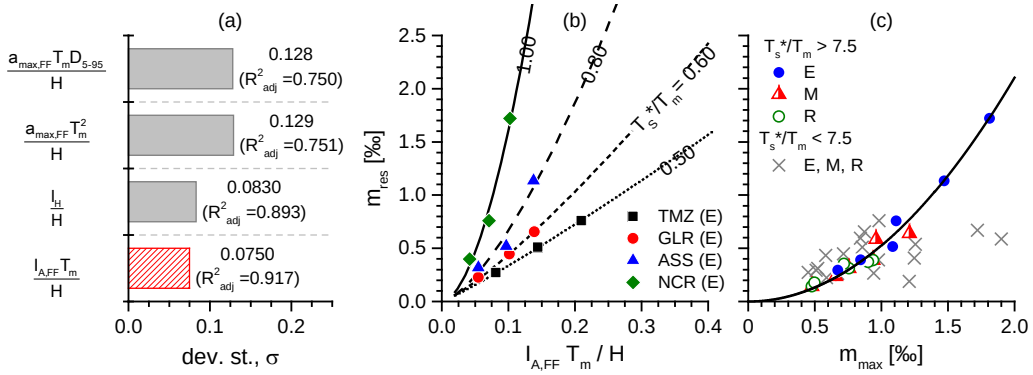

Figure 6. Standard error, σ, of data regression for different dimensionless IM parameters (a). Normalized residual bending moment, m_{res}, vs normalized Arias intensity condition and period ratio for natural records (E) (n_{eq}>10) (b). Normalized residual vs maximum moment (c).

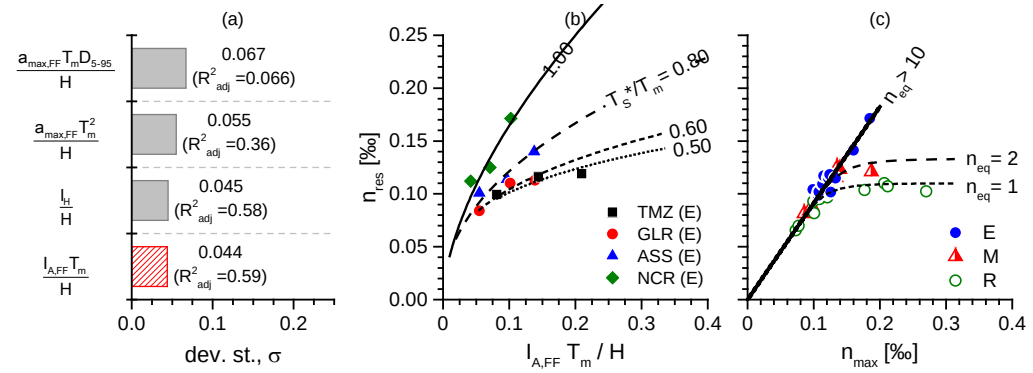

Figure 7. Standard error, σ, of data regression for different dimensionless IM parameters (a). Normalized residual axial load, n_{res}, vs normalized Arias intensity in free field condition and period ratio for natural records (E) (n_{eq}>10) (b). Normalized residual vs maximum axial load (c).

This correlation is shown in Figure 6b which reports m_{res}, defined here as the increment of the bending moment in post-seismic state normalised by the bending stiffness of the wall, *EI/H*, as a function of $I_{A,FF}$ (normalised by H/T_m) and of T_s^*/T_m for natural records (n_{eq}>10). Very well defined trends were also found for R and M waveforms. In the same way, Figure 7b refers to n_{res}, defined here as the increment of the axial load of the bottom prop in the post-seismic state normalised by the axial stiffness of the prop, *EA/L*. The influence of motion parameters $I_{A,FF}$, T_m, n_{eq} and of the fundamental soil period T_s^* on the value of post-seismic structural forces is clearly apparent. Regarding the maximum increments of structural actions during seismic motion, the interpretation of results is very complex. Maximum and post-seismic actions are supposed to be related; in Figure 6c, the normalised increments of maximum, m_{max}, and post-seismic, m_{res}, bending moments are plotted. The Figure 6c shows that a well-defined relationship exists only for the ASS and NCR waveforms (significant frequency content in the resonant range of the second vibration mode). A better correlation between maximum and post-seismic values was found for axial load in the bottom prop. The results shown in Figure 7b highlight, also, the effects of the number of equivalent loading cycles.

Conclusions

In this paper the preliminary results of a number of dynamic analyses in the time domain of a pair of multi-propped retaining walls that support an excavation in a dry coarse-grained soil excited by seismic loading have been presented and discussed. Soil model is characterized by a stress-dependent stiffness and a highly non-linear behaviour. Four acceleration time histories of strong-motion, characterized by a similar Arias intensity and significant duration but by different frequency contents have been used. 'Equivalent' analytical simple signals that characterize the peak pulse of the natural records were also considered.

The results of the analyses indicate a very complex response of the system, due to the effects of local seismic response and soil-structure interaction phenomena. This complexity is particular apparent in the interpretation of trend and magnitude of soil stresses acting on the walls. However, the analysis of the resulting actions on structural elements seems to highlight the ground motion characters that mainly influence the increase of these actions. In detail, the effect of the frequency content of the seismic input, compared to the fundamental frequencies of the soil profile and to the geometry of the system, appears to be dominant. Furthermore, the increase of structural actions appears to be a function of the number of cycles of the seismic input and of the motion at ground level in free field conditions, expressed in terms of Arias intensity. The latter has proven to be the most efficient parameter in the description of the relationship between ground motion parameters and seismic structural response as defined within the current performance-based design approaches.

References

Callisto L., Soccodato F.M. Seismic analysis of an embedded retaining structure in coarse-grained soils. *Proc. 4th Int. Conf. on Earthquake Gotechnical Engineering*. 25-28 June, 2007.Thessaloniki.

Callisto L., Soccodato F.M. Seismic design of cantilevered retaining walls. *Journal of Geotech. and Geoenv. Eng,*

2010. **136**(2): 344-354.

Conti, R., Madabhushi, G.S.P., Viggiani, G.M.B. On the behaviour of flexible retaining walls under seismic actions. *Geotechnique*, 2012, 62. pp. 1081-1094.

Itasca Consulting Group Inc. *Fast Lagrangian Analysis of Continua. User's Guide*. 5th Edition (FLAC Version 7.0) September 2011.

Kloukinas P., Langousis M., Mylonakis G. Simple Wave Solution for Seismic Earth Pressures on Nonyielding Walls. *J. Geotech. Geoenviron. Eng*., 2012, **138**(12): 1514–1519.

Kuhlemeyer R. L., Lysmer J. Finite Element Method accuracy for wave propagation problems. *Journal of Soil Mechanics & Foundations Division*, 1973, ASCE, **99**(SM5): 421-427.

Seed H.B., Idriss I.M. *Soil moduli and damping factors for dynamic analysis*. Report No. EERC 70-10, University of California, Berkeley, 1970.

Tothong, P, and Luco, N.. Probabilistic seismic demand analysis using advanced ground motion intensity measures. *Earthquake Engineering and Structural Dynamics*, 2007, **36** (13), 1837–1860.

Tropeano G., Soccodato F.M. Dynamic analyses of propped retaining structures. Proc. 8th European Conf. on *Numerical Methods in Geotechnical Engineering* (NUMGE 2014), 2014, 2, pp. 1193-1198.

Veletsos A. S., Younan A. H. Dynamic soil pressures on rigid vertical walls. *Earthquake Eng. Struct. Dyn*. 1994, **23**: 275–301

Wood J. H. *Earthquake-induced Soil pressures on Structures.* Ph.D thesis, The California Institute of Technology, Pasadena: California, 1973